HIGH-WAVENUMBER SOLAR f-MODE STRENGTHENING PRIOR TO ACTIVE REGION FORMATION

Nishant K. Singh[1], Harsha Raichur[1], & Axel Brandenburg[1,2,3,4]

[1]Nordita, KTH Royal Institute of Technology and Stockholm University, Roslagstullsbacken 23, SE-10691 Stockholm, Sweden
[2]JILA and Department of Astrophysical and Planetary Sciences, University of Colorado, Boulder, CO 80303, USA
[3]Department of Astronomy, AlbaNova University Center, Stockholm University, SE-10691 Stockholm, Sweden
[4]Laboratory for Atmospheric and Space Physics, University of Colorado, Boulder, CO 80303, USA

January 5, 2016, Revision: 1.110

ABSTRACT

Using the solar surface mode, i.e. the f-mode, we attempt to predict the emergence of active regions (ARs) in the days before they can be seen in magnetograms. Our study is motivated by earlier numerical findings of Singh et al. (2014) who showed that, in the presence of a nonuniform magnetic field which is concentrated a few scale heights below the surface, the f-mode fans out in the diagnostic $k\omega$ diagram at high wavenumbers. Here we exploit this property using data from the *Helioseismic and Magnetic Imager* aboard the *Solar Dynamics Observatory*, and show for three ARs 11768, 11158 and 12051, that at large latitudinal wavenumbers (corresponding to horizontal scales of around 3000 km), the f-mode displays strengthening about two days prior to AR formation and thus provides a new precursor for AR formation. The idea that the f-mode is perturbed days before any visible magnetic activity occurs on the surface can be important in constraining dynamo models aiming at understanding the global magnetic activity of the Sun.

Subject headings: Sun: dynamo – Sun: helioseismology – Sun: surface magnetism – turbulence

1. INTRODUCTION

Recent work has demonstrated the potential usefulness of employing the surface or fundamental f-mode in local helioseismology for detecting subsurface solar magnetism (Hanasoge et al. 2008; Daiffallah et al. 2011; Felipe et al. 2012, 2013). While turbulence generally tends to lower the f-mode frequency relative to its theoretical value (Fernandes et al. 1992; Murawski & Roberts 1993a; Duvall et al. 1998) given by $\omega_f = \sqrt{gk}$, where g is the gravitational acceleration and k is the horizontal wavenumber, horizontal magnetic fields can increase the frequency (Murawski & Roberts 1993b) and vertical or inclined fields lead to a nonuniform behavior, depending on the value of the horizontal wavenumber (Singh et al. 2015). More importantly, however, horizontal variability of the subsurface magnetic field leads to a fanning of the f-mode, where changes in the integrated mode amplitude and position give clues about the depth of such a field (Singh et al. 2014). While these investigations demonstrated a number of previously unknown effects of the f-mode, they were restricted to idealizing conditions of an isothermal layer. In the present Letter, we use observations with the *Helioseismic and Magnetic Imager* (HMI) aboard the *Solar Dynamics Observatory* to search for possible similarities between observations and simulations.

We focus in particular on the possibility of using changes in the f-mode to predict the emergence of active regions (ARs) days before they can be seen in magnetograms. Owing to the very nature of the f-mode being confined to the proximity of the surface, our approach appears to be most sensitive to magnetic fields at shallow depths of just a few megameters (Mm), and ceases to be sensitive when the AR begins to become fully developed. Earlier attempts of predicting the emergence of ARs

employed time-distance seismology using p-modes and have suggested the occurrence of perturbations at larger depths of 40–75 Mm (Ilonidis et al. 2011; Kholikov 2013). On the other hand, the rising flux tube scenario suggests a retrograde flow at a depth of 30 Mm (Birch et al. 2010), which has however not been observed. By contrast, in the distributed dynamo scenario (Brandenburg 2005), magnetic flux concentrations form spontaneously near the surface (Brandenburg et al. 2011, 2013), which might explain the aforementioned field concentrations at shallower depths. Spontaneous surface flux concentrations have also been seen in the deep hydromagnetic convection simulations of Stein & Nordlund (2012), where an unstructured magnetic field is allowed to enter the bottom of their computational domain. Such near-surface magnetic concentrations are expected to affect the f-mode as its eigenfunction peaks only a few Mm below the solar surface (cf. Schou 1999). It is possible that these perturbations could manifest themselves through detectable signatures.

Readers familiar with the conventional picture of buoyant flux tube emergence (e.g., Charbonneau 2010) might be concerned about depths as shallow as just a few Mm, because buoyant tubes of several kilogauss would reach the surface within an hour (~ 3 hours from the depth of 7.5 Mm in the simulations of Cheung et al. 2010), but this model ignores the formation process and implants flux tubes as alien objects within the turbulent convection zone. By contrast, ARs and sunspots might instead be generated by the subsurface turbulence in ways similar to what has so far only been seen in rather idealized simulations (Brandenburg et al. 2013; Warnecke et al. 2013; Mitra et al. 2014). The point here is not to defend this idea, but to raise the awareness of alternative viewpoints that would facilitate the understanding of our results presented below.

Once the AR has been detected in magnetograms and

Electronic address: nishant@nordita.org

becomes fully developed, the mode amplitude begins to be suppressed. This might be explained by the fact that the interaction of both f- and p-modes with ARs or sunspots leads to mode conversion, resulting in the absorption of mode power (Thomas, et al. 1982; Cally et al. 1994; Cally & Bogdan 1997). This would explain the observed reduction of the mode amplitude *after* the analyzed AR has been formed. However, what was not discussed earlier is that the mode amplitude from the same region can undergo a transient growth phase prior to the actual flux emergence. This exhibits an interesting non-monotonic temporal variation in the normalized mode power, which first rises, reaches a maximum value a few days before there is any sign of flux emergence, and then decreases as the strength of the magnetic field in the same region increases. Although a proper explanation of this is not yet available, one might speculate that this could also be due to some kind of scattering, whereby p-modes would scatter off the magnetic flux concentrations and leak into enhanced f-mode power.

2. DATA ANALYSIS

We use line-of-sight Dopplergram and magnetogram data from observations with HMI in the cylindrical equal-area projection mappings that are publicly available on the Stanford website[1]. Our analysis is based on 45 seconds cadence data with a projection scale of $0.03°$ per pixel, where the data represent the line-of-sight Doppler velocity $v(x, y, t)$. For each of the regions of interest, we consider a patch of 512^2 pixels covering an area of about $(180\,\mathrm{Mm})^2 \approx (15°)^2$ on the solar surface. We track these patches for several days using a frame of reference corotating with the mean (Carrington) rotation rate Ω_0 with $\Omega_0/2\pi = 424\,\mathrm{nHz}$. In order to capture transient signatures, we use data cubes $v(x, y, t)$ of only 8 hours duration for the entire tracking period of our target region. To reduce the noise level arising from solar convection (Zhao et al. 2015) and effects from latitudinal differential rotation (J. Zhao, private communication), we use a running difference to the original images before storing $v(x, y, t)$.

We divide our five or six day stretches into 15 or 18 stretches of 8 hrs, each with 45 secs cadence, resulting in a data cube of $512^2 \times 640$ points of $v(x, y, t)$ that is Fourier transformed to give $\hat{v}(k_x, k_y, \omega)$. We then construct power spectra from $P = |\hat{v}|^2$ and select $k_x = 0$ in the subsequent analysis. Thus, we ignore longitudinal variations that would be affected by the cylindrical equal-area projection, because the latitudinal directions are expected to be the least affected. Also, our target regions were chosen such that the patches were always far from the limb during the entire tracking period. The thus obtained power spectra $P(k_x = 0, k_y, \omega)$ are then used to construct a diagnostic $k\omega$ diagram in the k_y-ω plane; see Fig. 1(a) which displays the f- and p-ridges where the horizontal wavenumber is $k = k_y$.

We now take a cut parallel to the frequency axis at a fixed $k_y R_\odot$ to get the line profiles of the f- and lowest two p-ridges. We then apply a boxcar smoothing along the frequency axis with a box width of $0.24\,\mathrm{mHz}$. To determine the strength of the f-mode, which lies approximately at $\omega = \sqrt{gk}$, where $g = 274\,\mathrm{m\,s^{-2}}$ is the solar

surface gravity, we remove the continuum and the lowest two p-ridges, which are represented by a superposition of parabolic and Gaussian/Lorentzian fits, respectively and denoted by $P_{\mathrm{cp}} = |\hat{v}|^2_{\mathrm{cp}}$, where the subscript cp stands for the sum of continuum and p-modes; see Fig. 1(b) and (c). Repeating the same procedure at all wavenumbers in the range mentioned later, we find the f-mode power as $P_f(k_y, \omega) = |\hat{v}_f|^2 = P - P_{\mathrm{cp}}$. We may define the integrated f-mode amplitude as

$$\langle v^2 \rangle_f = 2AT \int_0^\infty \int_0^\infty k_y P_f(k_y, \omega) \frac{\mathrm{d}k_y}{2\pi} \frac{\mathrm{d}\omega}{2\pi} \quad (1)$$

which we write as

$$\langle v^2 \rangle_f = L \sum_{k_y} k_y P_{f,k_y} \text{ with } P_{f,k_y} = 2 \sum_\omega P_f(k_y, \omega), \quad (2)$$

where $A = L^2$ is the area of the chosen patch, L is the side length and T is the tracking time of the data cube. Thus, we can determine the energy of the f-mode, E_f, characterizing its strength, as:

$$E_f(t) \equiv \frac{1}{2} \langle v^2 \rangle_f(t) = \frac{1}{2} \left(\frac{L}{R_\odot} \right) \sum_{k_y} \psi(k_y) \quad (3)$$

with $\psi(k_y) = k_y R_\odot P_{f,k_y}$; see Fig. 1(d) and (e). The time dependence of E_f may now be determined by computing the above quantities from the sequence of 8 h data cubes prepared for all tracked regions of interests.

In the quiet phase, say, during solar minimum, quantities such as E_f show a modulation as the tracked region passes the central meridian, with its maximum coinciding with the time corresponding to the central meridian passage, denoted as $\Delta t^{\mathrm{CM}} = 0$. The dominant contribution to this modulation comes from the cosine of the angular distance α to disk center, which is given by

$$\cos\alpha = \cos\vartheta \cos\varphi; \quad \varphi = \varphi_* - \varphi_0 + \Omega_{\mathrm{syn}} t, \quad (4)$$

with ϑ and φ being respectively the latitude and longitude of the point of interest, φ_* is the corresponding Carrington longitude, φ_0 is the Carrington longitude of the disk center at the time when we began tracking the target patch, and $\Omega_{\mathrm{syn}} = 2\pi/27.275\,\mathrm{days}$ is the mean synodic Carrington rotation rate of the Sun (i.e., the apparent rotation rate as viewed from the Earth). We find it useful to show the evolution of the quantity $\widetilde{E}_f = E_f/\cos\alpha$ computed from various regions of interests.

As suggested by earlier work (Singh et al. 2014), we focus on the integrated f-mode amplitude, E_f, for fairly large latitudinal wavenumbers, k_y. We track a particular position on the solar surface in time t using the average (Carrington) rotation rate. Normalizing by the solar radius $R_\odot = 700\,\mathrm{Mm}$ gives the spherical harmonic degree $k_y R_\odot$. For a fixed range of $k_y R_\odot \in [1100, 1500]$, we compute the dependence of E_f on t. Empirically, the value of E_f of the quiet Sun (the position where no AR emerges within the next few days) shows a systematic $\cos\alpha$ dependence with distance α from the center of the solar disk. Thus, $\widetilde{E}_f \equiv E_f/\cos\alpha$ is found to be nearly independent of α in the quiet phase of the Sun. However, several days *prior* to the emergence of an AR, our studies show elevated values of $\widetilde{E}_f$ at that corotating patch where this AR later emerges.
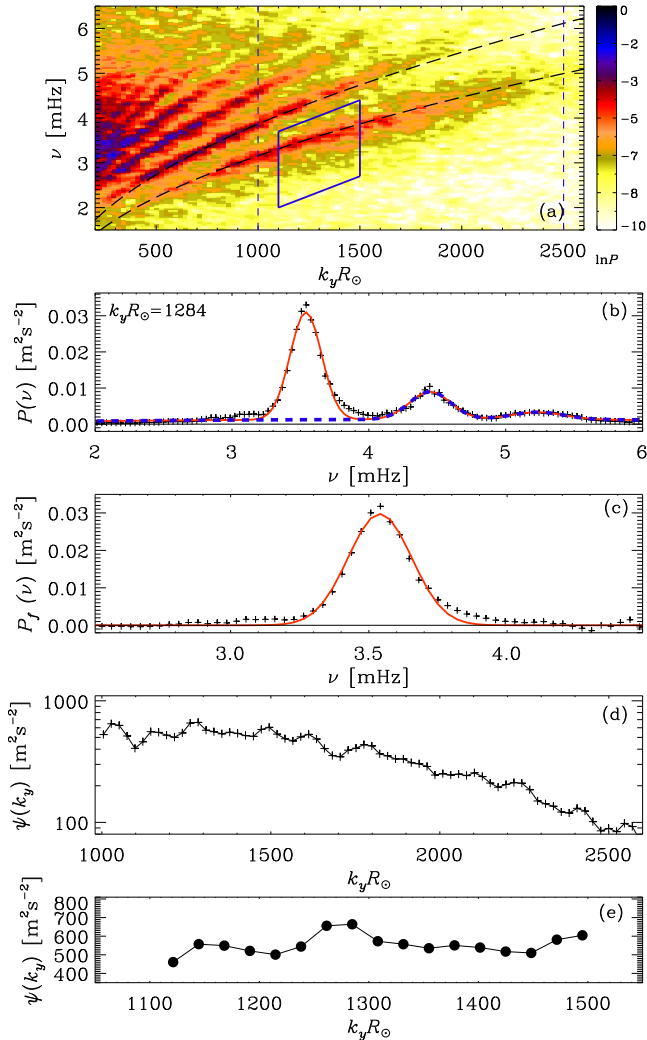
FIG. 1.— (a) Typical $k\omega$ diagram where the lowest ridge is the f-mode; (b) example of a vertical cut at a specified $k_y R_\odot$ (plus symbols) together with the model fit (solid, red curve) and P_{cp} (dashed, blue line); (c) f-mode ridge (P_f, plus symbols) and the corresponding fit (solid, red curve); (d) $\psi(k_y)$ for the full range enclosed within the vertical dashed lines in (a); (e) $\psi(k_y)$ for the range of $k_y R_\odot$ used to determine E_f, see the parallelogram of (a).

For the purpose of reliably identifying on the solar disk potential localized regions which are going to show ARs, it is necessary to make a simultaneous comparison with the behavior of relatively quiet Sun patches under otherwise identical local conditions. This benchmarking may be realized as follows: corresponding to each target region at (ϑ, φ), we consider a mirror (quiet) region at $(\vartheta^\dagger, \varphi)$ in the opposite hemisphere with the same dimensions, and track both these patches simultaneously, where $\vartheta^\dagger = -\vartheta$ for the entire tracking period. This, however, would be ideal if only one of the two such patches show an AR and/or if they are not too close to the equator and therefore non-overlapping. The temporal behavior of $\widetilde{E}_f$ obtained from a quiet Sun patch lying at an arbitrary location offers yet another comparison. This assumes that $\widetilde{E}_f(\alpha)$ is expected to be nearly flat for the quiet Sun patch. For ARs 11768 and 11158, we utilize the former technique in terms of $\vartheta^\dagger$, whereas for the AR 12051 we use the latter approach in terms of a similar position to assess the presence and significance of the precursor signal.

For ARs 11768 and 11158, we compute $\widetilde{E}_f$ and $\widetilde{E}_f^\dagger$ (computed from the corresponding mirror point in the opposite hemisphere), to simultaneously demonstrate their evolutions. We also monitor the differences in the f-mode energies from the two (active and corresponding quiet) regions as function of time. Unless otherwise specified, we denote such a difference by $\Delta\widetilde{E}_f = \widetilde{E}_f - \widetilde{E}_f^\dagger$. For AR 12051, we consider two quiet Sun regions at $\vartheta = +25°$ and $-35°$, which were tracked for the same time period as that of the AR, with identical φ. The f-mode energies computed from these quiet regions are denoted by $\widetilde{E}_{f(+25)}$ and $\widetilde{E}_{f(-35)}$, with corresponding energy differences being $\Delta\widetilde{E}_{f(+25)} = \widetilde{E}_f - \widetilde{E}_{f(+25)}$ and $\Delta\widetilde{E}_{f(-35)} = \widetilde{E}_f - \widetilde{E}_{f(-35)}$, respectively.

3. RESULTS

In Fig. 2 we show magnetograms and the time trace for a corotating patch at which later an AR emerged: left column for AR 11768, middle one for AR 11158, and right one for AR 12051. Although AR 11768 was designated its number only on 2013 June 13 (denoted by time $t = t_{AR}$ in the figures), the local value of $\widetilde{E}_f$ reached a maximum with specific energy difference of the order of ~ 100 m^{2}s^{-2} relative to the corresponding quiet Sun region from the opposite hemisphere. Such a local strengthening of the f-mode is seen almost three days before AR 11768 finally emerged and about two days before the rms magnetic field, B_{rms}, reaches a plateau of about 90 G within the considered patch. It is intriguing to note the subsequent strengthening of the f-mode at the neighboring quite Sun region, which is possibly due to a causal response at a distant location, as these seismic signals may well be nonlocal. This AR produced several C-class flares during June 14–17 before it disappeared on the western limb on June 17.

Next, we consider AR 11158, which was a rapidly growing AR that produced the first X-class flare of solar cycle 24 on 2011 February 15 (Maurya et al. 2012) with an Earth-directed halo coronal mass ejection (Schrijver et al. 2011). It also produced several M-class flares during February 13–16 (Inoue et al. 2013), after being designated its number on February 12. Also in this case, $\widetilde{E}_f$ shows a clear increase with $\Delta\widetilde{E}_f \sim 200$ m^{2}s^{-2} about a day before B_{rms} reaches a plateau of about 220 G, as may be seen from the second column of Fig. 2. The energy increase seen about three days prior to the AR emergence appears to be indicative of the subsurface concentration of the magnetic field resulting in a rapid growth of B_{rms} at the photosphere. Thus, the same general trend is found here too, although the potential for using $\widetilde{E}_f(t)$ as a precursor was less strong in the sense that it showed the signal only about a day in advance, but with twice an energy increase compared to the AR 11768. The possible causal response at the corresponding quiet Sun location is noticeable here as well, contributing to the negative values of $\Delta\widetilde{E}_f$ after the magnetic flux emergence on the photosphere; see the second column of Fig. 2.

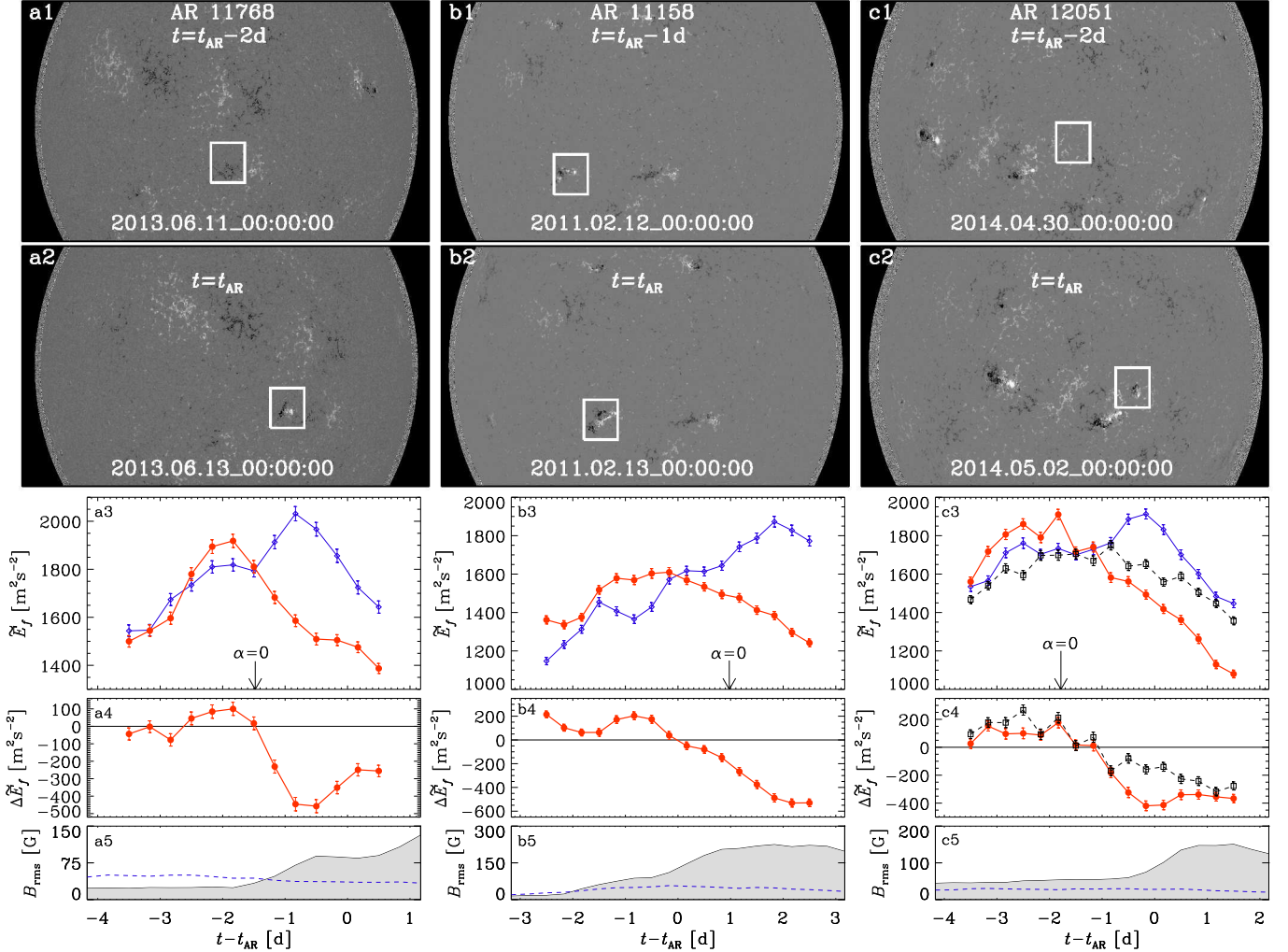Finally, we compare $\widetilde{E}_f$ for AR 12051 with that of

FIG. 2.— From left to right for ARs 11768, 11158, and 12051: (a1)–(c1) magnetograms 1–2 days before t_{AR}; (a2)–(c2) same as above, but at $t = t_{\mathrm{AR}}$; (a3)–(c3) evolution of $\widetilde{E}_f$ corresponding to ARs (red) and their mirror regions (blue) except for (c3), where blue and black curves show evolution of $\widetilde{E}_{f(+25)}$ and $\widetilde{E}_{f(-35)}$, respectively; (a4)–(c4) evolution of $\Delta\widetilde{E}_f$ but in (c4) red and black curves show the evolution of $\Delta\widetilde{E}_{f(+25)}$ and $\Delta\widetilde{E}_{f(-35)}$, respectively; (a5)–(c5) gray shaded regions show growth of B_{rms} of respective AR and the dashed blue curves show B_{rms} of the mirror region, except in (c5) where the curve shows the evolution of B_{rms} at $\vartheta = +25°$.

two neighboring quiet Sun patches; see the last column of Fig. 2. Just like the other two examples presented above, the local strength of the f-mode, obtained from the patch which later shows AR 12051, is larger compared to the corresponding quiet Sun patches, showing a significant energy increase of the order of $\sim$150 m²s⁻² more than two days before it was designated its number on 2014 May 2 and nearly three days before B_{rms} reached its maximum value of about 150 G. On May 3, this AR developed a so-called δ-class spot with M class flares a few days later, but by that time the flare no longer faced the Earth to pose any threat. Note that δ spots have opposite polarities within a common penumbra and are not easily explained within the rising flux-tube scenario, but are a natural outcome within scenarios where spots are produced spontaneously near the surface (Mitra et al. 2014).

All three examples presented above show that several days prior to magnetic field emergence the strength of the f-mode, as presented by the value of $\widetilde{E}_f$, increases above its usual value obtained from the corresponding

quiet Sun location. We also note that the energy increase $\Delta\widetilde{E}_f > 0$ prior to AR formation appears to be directly proportional to the final strength of the magnetic field when the AR is fully developed. Thus, while the details vary for different ARs, the qualitative similarity between all of them is remarkable: strengthening of the f-mode at a local patch where later an AR develops. This suggests that $\widetilde{E}_f$ might be a robust precursor to AR formation. As a control, we now consider a co-moving patch during 2010, when the Sun was near solar minimum and no AR emerged within and around the chosen patch. As expected, the resulting time trace of $\widetilde{E}_f$ (Fig. 3) is essentially flat and fluctuating around its base value, $\widetilde{E}_{f0} = 1750\,\mathrm{m}^2\,\mathrm{s}^{-2}$.

It would be interesting to see whether there are other indicators, for example in the magnetic field itself, which could also give early indications of AR formation. We emphasize, however, that the maximum of $|B|$ shows an onset only at the same time as B_{rms} does, which is therefore too late. An important extension of the present work
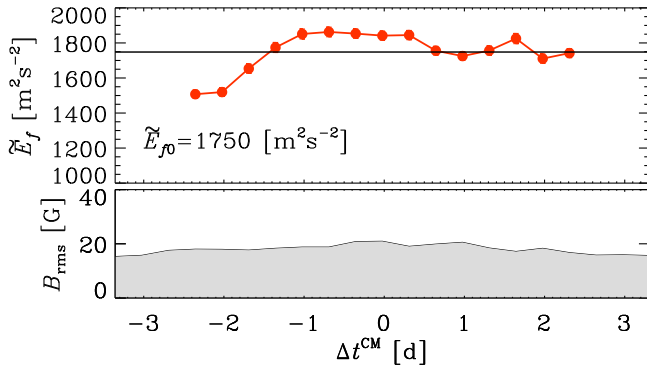
FIG. 3.— $\widetilde{E}_f$ and $B_{\rm rms}$ for comoving patch during an arbitrarily chosen time interval during 2010 when solar activity was low over the entire disk. Here, $\Delta t^{\rm CM}$ denotes the time with respect to the moment when the patch was crossing the central meridian. The solid horizontal line marks the average value, $\widetilde{E}_{f0} = 1750\,{\rm m}^2\,{\rm s}^{-2}$.

would be to calculate an image of $\widetilde{E}_f$ for the full solar disk. This would give most direct information of where the next AR might form. Determining a possible functional dependence of the pre-emergence energy difference $\Delta\widetilde{E}_f$ on the strength of the magnetic field when the AR becomes fully developed would also be important. Based on the three ARs studied here, this correlation seems to be positive, but we need to analyze a much larger sample of ARs to learn further. We envisage that the monitoring of the f-mode energy from an array of localized patches, together with an approach presented by Amari et al. (2014) to assess the complexity/twist of the global magnetic structures, might allow us to say which AR develops an Earth-bound CME.

4. IMPLICATIONS

If we accept that $\widetilde{E}_f(t)$ can be used as a precursor to AR formation, we must ask about its possible physical origin and relevance. Earlier idealized simulations (Singh et al. 2014, 2015) have demonstrated that, while uniform magnetic fields lead to a frequency shift and a weakening of the f-mode, a nonuniform subsurface field can lead to a fanning and associated strengthening of the f-mode, provided the magnetic field is at least one or two pressure scale heights below the surface. While such studies should be repeated with more realistic models, they do confront us with the question of how a magnetic field can remain undetected once it is only a few Mm below the surface.

The fact that the f-mode resides near the top few Mm of the Sun, is suggestive of a gradual build-up of the AR near the surface, instead of a buoyant rise, which would happen in just a few hours (Cheung et al. 2010). This is in stark contrast to the conventional picture of an Ω-shaped flux tube rising from the bottom of the convection zone and forming an AR as it pierces the surface (Fan 2001). Earlier simulations of Cheung et al. (2010) with a magnetic field implanted at a depth of nearly 10 Mm below the surface have produced surface manifestations just a few hours later. Such simulations do not address the physics of the *formation* of magnetic flux concentrations. By contrast, several simulations in large enough domains performed by several groups (Stein & Nordlund 2012; Warnecke et al. 2013; Mitra et al. 2014) have demonstrated the spontaneous emergence of magnetic flux concentrations right at the surface. This highlights the potential significance of f-mode related precursors for constraining our still very sketchy understanding of the solar dynamo (Ossendrijver 2003; Brandenburg 2005; Charbonneau 2010).

REFERENCES

Amari, T., Canou, A., & Aly, J.-J. 2014, Nature, 514, 465
Birch, A. C., Braun, D. C., & Fan, Y. 2010, ApJ, 723, L190
Brandenburg, A. 2005, ApJ, 625, 539
Brandenburg, A., Kemel, K., Kleeorin, N., Mitra, D., & Rogachevskii, I. 2011, ApJ, 740, L50
Brandenburg, A., Kleeorin, N., & Rogachevskii, I. 2013, ApJ, 776, L23
Cally, P. S., Bogdan, T. J., & Zweibel, E. G. 1994, ApJ, 437, 505
Cally, P. S., & Bogdan, T. J. 1997, ApJ, 486, L67
Charbonneau, P. 2010, Living Rev. Solar Phys., 7, 3
Cheung, M. C. M., Rempel, M., Title, A. M., & Schüssler, M. 2010, ApJ, 720, 233
Daiffallah, K., Abdelatif, T., Bendib, A., Cameron, R., & Gizon, L. 2011, Solar Phys., 268, 309
Duvall, T. L., Jr., Kosovichev, A. G., & Murawski, K. 1998, ApJ, 505, L55
Fan, Y. 2001, ApJ, 554, L111
Felipe, T., Braun, D., Crouch, A., & Birch, A. 2012, ApJ, 757, 148
Felipe, T., Crouch, A., & Birch, A. 2013, ApJ, 775, 74
Fernandes, D. N., Scherrer, P. H., Tarbell, T. D., & Title, A. M. 1992, ApJ, 392, 736
Hanasoge, S. M., Birch, A. C., Bogdan, T. J., & Gizon, L. 2008, ApJ, 680, 774
Ilonidis, S., Zhao, J., & Kosovichev, A. 2011, Science, 333, 993
Inoue, S., Hayashi, K., Shiota, D., Magara, T., & Choe, G. S. 2013, ApJ, 770, 79

Kholikov, S. 2013, Solar Phys., 287, 229
Maurya, R. A., Vemareddy, P., & Ambastha, A. 2012, ApJ, 747, 134
Mitra, D., Brandenburg, A., Kleeorin, N., Rogachevskii, I. 2014, MNRAS, 445, 761
Murawski, K. and Roberts, B. 1993a, A&A, 272, 601
Murawski, K. and Roberts, B. 1993b, A&A, 272, 595
Ossendrijver, M. 2003, A&A Rev., 11, 287
Schou, J. 1999, ApJ, 523, L181
Schrijver, C. J., Aulanier, G., Title, A. M., Pariat, E., & Delannée, C. 2011, ApJ, 738, 167
Singh, N. K., Brandenburg, A., & Rheinhardt, M. 2014, ApJ, 795, L8
Singh, N. K., Brandenburg, A., Chitre, S. M., & Rheinhardt, M. 2015, MNRAS, 447, 3708
Stein, R. F., & Nordlund, Å. 2012, ApJ, 753, L13
Thomas, J. H., Cram, L. E., & Nye, A. H. 1982, Nature, 297, 485
Warnecke, J., Losada, I. R., Brandenburg, A., Kleeorin, N., & Rogachevskii, I. 2013, ApJ, 777, L37
Zhao, J., Chen, R., Hartlep, T., & Kosovichev, A. G. 2015, ApJ, 809, L15